Numerical Investigation of a Complete Scramjet Demonstrator Model for Experimental Testing Under Flight Conditions

Yann Simsont, Peter Gerlinger, and Manfred Aigner

Abstract In the present paper a complete scramjet demonstrator model for experimental testing at Mach 8 is investigated numerically using the scientific code TASCOM3D (Turbulent All Speed Combustion Multigrid Solver) on the HPC vector system NEC SX-9, installed at the High Performance Computing Center Stuttgart (HLRS). First the three-dimensional intake of the model is simulated. Then the results are used as inlet conditions for the simulation of the combustor, where hydrogen is injected by a lobed strut injector located in the middle of the diverging chamber. The test conditions, corresponding to a flight speed of Mach 8 at an altitude of 30 km, and the results of the simulations are discussed in detail, occurring difficulties are highlighted. In order to ensure self-ignition and prevent the flow from blockage, potential design changes are described and investigated in order to proof their functionality. Finally the performance of the reactive and non-reactive simulations on the NEC SX-9 is analyzed.

1 Introduction

For future hypersonic transportation the use of air breathing engines (i.e. ramjets for flight Mach numbers 2–7 and scramjets for flight Mach numbers 5–15) is of great interest. Contrary to rocket driven systems no oxygen is transported. Therefore air breathing engines provide the opportunity to increase the payload to total mass ratio, and thus reduce the cost per payload unit. The main objective of the Research Training Group GRK 1095/2 (University of Stuttgart, Technical University of Munich, RWTH Aachen University and DLR Cologne) is the design and development of a complete scramjet demonstrator model. Experimental testing of the model is

Y. Simsont (✉) · P. Gerlinger · M. Aigner
Institut für Verbrennungstechnik der Luft- und Raumfahrt, Universität Stuttgart, Pfaffenwaldring 38-40, 70569 Stuttgart, Germany
e-mail: yann.simsont@dlr.de

W.E. Nagel et al. (eds.), *High Performance Computing in Science and Engineering '12*,
DOI 10.1007/978-3-642-33374-3_15,

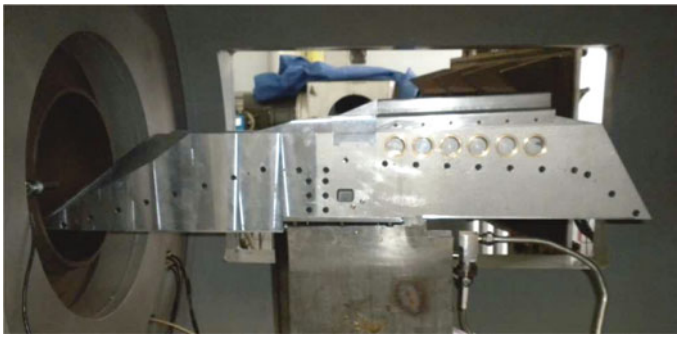

Fig. 1 Scramjet demonstrator model in the hypersonic test facility IT-302

funded by the DFG grant GA 1332/1-1 and conducted in two hypersonic wind tunnels (IT-302 and AT-303) at the Khristianovich Institute of Theoretical and Applied Mechanics (ITAM), Russian Academy of Sciences, Siberian Branch in Novosibirsk, Russia. A first testing period has been accomplished in October and November 2011, a second testing period has been performed in March and April 2012. Figure 1 shows the complete scramjet demonstrator model mounted in the IT-302 wind tunnel. In the present paper the final numerical simulations before experimental testing are described. Those simulations are directed at distinguishing unfavorable flow conditions, which might occur during testing (e.g. blockage of the intake, deficient self-ignition in the combustor, thermal blockage, etc.), as well as suitable correctives to avoid those phenomena and ensure successful experiments. In respect of the advanced stage of the project – the scramjet demonstrator model had already been assembled – potential design modifications derived from the numerical results have to be easy to implement.

2 Geometry and Test Design

The investigated scramjet demonstrator model consists of an intake, an isolator, a combustor with central strut injection and a nozzle (Fig. 2) and has a total length of 1.046 m. The intake combines a single outer compression ramp (15.5° angle) and side wall compression (3.5° angle) and has been developed based on a 3D mixed compression intake tested at ITAM [1] and various numerical simulations [2]. Gaseous hydrogen is injected at $x = 623$ mm downstream of the ramp leading edge in axial flow direction at the trailing edge of a lobed strut injector through seven horizontal and six vertical ports shown in Fig. 3. The strut is mounted centrally in the model from one sidewall to the other and corresponds to previously investigated lobed strut injectors [3, 4]. The lobed structure creates streamwise vortices and therefore enhances the mixing of fuel and air. The combustion chamber has a rectangular cross section, the top and bottom walls diverge – each with an angle of 2° – beginning at $x = 580$ mm (at half length of the strut).

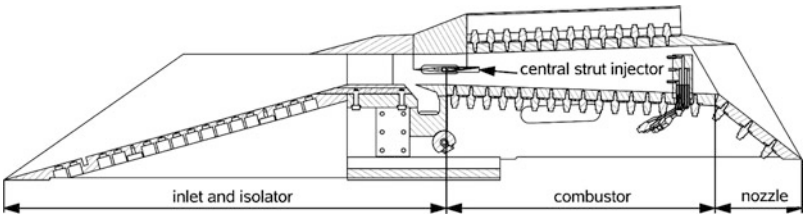

Fig. 2 Drawing of longitudinal section of the scramjet demonstrator model with instrumentation

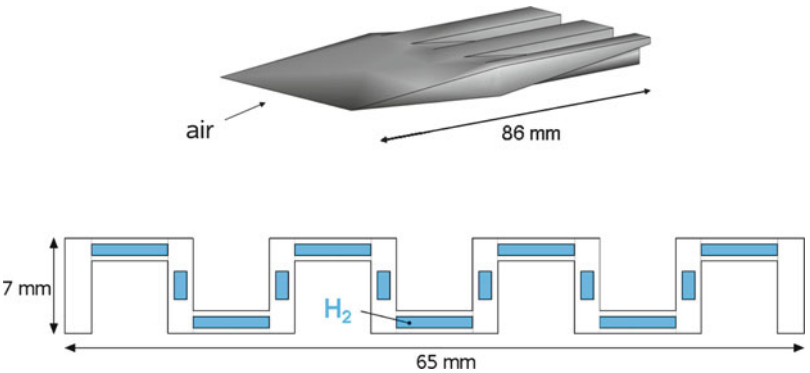

Fig. 3 Sketch of central lobed strut injector (*top*) and areas of hydrogen injection at the trailing edge of the injector highlighted in *blue* (*bottom*)

Table 1 Inflow conditions for experimental testing at Mach 8

Air conditions	A	B
Mach number Ma_∞ (−)	8	8
Velocity u_∞ ($\frac{m}{s}$)	2,472	2,201
Total pressure p_0 (bar)	110	110
Static pressure p_∞ (Pa)	1,127	1,127
Total temperature T_0 (K)	3,280	2,600
Static temperature T_∞ (K)	238	188
Wall temperature T_{wall} (K)	293	293

The intake ramp is equipped with 15 thermocouples and two static pressure transducers along the center line. Over 30 pressure transducers are integrated in the top and bottom wall of the combustor and a Pitot rake is mounted at the end of the combustor to measure the Mach number at 5 points of the cross section. The test conditions, corresponding to a flight speed of Mach 8 at an altitude of 30 km, are summarized in column A of Table 1. Column B lists the conditions for a lower total temperature T_0 also tested experimentally. Since the measurement duration in the wind tunnels is relatively short (about 100 ms) the wall temperature of the model is assumed to be constant. To benefit from the symmetry of the investigated scramjet model and economize computation time, only one half of the model is simulated using approximately 24 million structured grid cells (14.4 million for the intake and 9.6 million for the combustor).

3 Governing Equations and Numerical Scheme

The investigations presented in this paper are performed using the scientific code TASCOM3D. The code has been used successfully in the last two decades simulating reacting and non-reacting flows. It describes reacting flows by solving the full compressible Navier-Stokes, species and turbulence transport equations. Additionally an assumed PDF (probability density function) approach is used to take turbulence chemistry interaction into account. The set of averaged equations in three-dimensional conservative form is given by

$$\frac{\partial \mathbf{Q}}{\partial t} + \frac{\partial (\mathbf{F} - \mathbf{F}_v)}{\partial x} + \frac{\partial (\mathbf{G} - \mathbf{G}_v)}{\partial y} + \frac{\partial (\mathbf{H} - \mathbf{H}_v)}{\partial z} = \mathbf{S}\,, \tag{1}$$

where

$$\mathbf{Q} = \left[\bar{\rho}, \bar{\rho}\tilde{u}, \bar{\rho}\tilde{v}, \bar{\rho}\tilde{w}, \bar{\rho}\tilde{E}, \bar{\rho}q, \bar{\rho}\omega, \bar{\rho}\sigma_T, \bar{\rho}\sigma_Y, \bar{\rho}\tilde{Y}_i\right]^T, \quad i = 1, 2, \ldots, N_k - 1\,. \tag{2}$$

The variables in the conservative variable vector $\mathbf{Q}$ are the density $\bar{\rho}$ (averaged), the velocity components (Favre averaged) $\tilde{u}$, $\tilde{v}$ and $\tilde{w}$, the total specific energy $\tilde{E}$, the turbulence variables $q = \sqrt{k}$ and $\omega = \epsilon / k$ (where k is the kinetic energy and ϵ the dissipation rate of k), the variance of the temperature σ_T and the variance of the sum of the species mass fractions σ_Y and finally the species mass fractions $\tilde{Y}_i$ ($i = 1, 2, \ldots, N_k - 1$). Thereby N_k describes the total number of species that are used for the description of the gas composition. The vectors $\mathbf{F}$, $\mathbf{G}$ and $\mathbf{H}$ specify the inviscid fluxes in x-, y- and z-direction, $\mathbf{F}_v$, $\mathbf{G}_v$ and $\mathbf{H}_v$ the viscous fluxes, respectively. The source vector $\mathbf{S}$ in Eq. (1) includes terms from turbulence and chemistry and is given by

$$\mathbf{S} = \left[0, 0, 0, 0, 0, \bar{S}_q, \bar{S}_\omega, \bar{S}_{\sigma_T}, \bar{S}_{\sigma_Y}, \bar{S}_{Y_i}\right]^T, \quad i = 1, 2, \ldots, N_k - 1\,, \tag{3}$$

where $\bar{S}_q$ and $\bar{S}_\omega$ are the averaged source terms of the turbulence variables, $\bar{S}_{\sigma_T}$ and $\bar{S}_{\sigma_Y}$ the source terms of the variance variables (σ_T and σ_Y) and $\bar{S}_{Y_i}$ the source terms of the species mass fractions. For turbulence closure a two-equation low-Reynolds-number q-ω turbulence model is applied [5]. The momentary chemical production rate of species i in Eq. (3) is given by

$$S_{Y_i} = M_i \sum_{r=1}^{N_r} \left[\left(\nu''_{i,r} - \nu'_{i,r}\right) \left(k_{fr} \prod_{l=1}^{N_k} c_l^{\nu'_{l,r}} - k_{br} \prod_{l=1}^{N_k} c_l^{\nu''_{l,r}} \right) \right], \tag{4}$$

where k_{f_r} and k_{b_r} are the forward and backward rate constants of reaction r (defined by the Arrhenius function), the molecular weight of a species M_i, the species concentration $c_i = \rho \tilde{Y}_i / M_i$ and the stoichiometric coefficients $\nu'_{i,r}$ and $\nu''_{i,r}$ of species i in reaction r. The averaged chemical production rate for a species i due

to the use of an assumed PDF approach is described in detail in Refs. [6, 7]. In the present paper the reactive simulations have been performed using a modified Jachimowski hydrogen/air reaction mechanism with 9 species and 19 steps [8, 9]. The unsteady set of differential equations in Eq. (1) is solved using an implicit lower-upper symmetric Gauss-Seidel (LU-SGS) [8, 10–12] finite-volume algorithm, where the finite-rate chemistry is treated fully coupled with the fluid motion. More details concerning TASCOM3D may be found in Refs. [7, 8, 12–14].

4 Investigation of the 3D Intake

In this section the three-dimensional intake and the subsequent isolator are investigated using the experimental test conditions listed in Table 1 in column A. The main focus is the generation of convenient flow conditions to enable self-ignition in the combustor while any blockage must be prevented. Figure 4 shows the Mach number distribution in the central plane of the model. The compression of the incoming air is effected by two strong shock waves: the first is the leading ramp shock which shortly misses the cowls lip, the second shock wave originates at the cowl and impinges on the thick boundary layer on the bottom wall of the model close to the central strut injectors leading edge. The interaction of the cowl shock and the boundary layer induces a separation zone with low Mach numbers shown in detail in the lower part of Fig. 4. Although the extent of the separation in the spanwise cross section is relatively small, the flow beneath the central strut injector is perturbed. In order to avoid the impingement of the cowl shock on the boundary layer a passive suction slot is added to the intake model at x = 525 mm.

To determine the size of the opening two different designs are investigated numerically. Suction I is 15 mm long and has an angle of 45° at the leading edge and 20° at the trailing edge, suction II is 25 mm long, has the same angle of 45° at the leading edge, though an angle of 37° at the trailing edge. The Mach number distribution in the central plane upstream of the strut is given for both slot configurations in Fig. 5. As intended suction I as well as suction II capture the cowl shock. Consequently the separation zone is successfully eliminated by the suction. Table 2 lists the air mass flows for the intake and the two suction slot configurations. The loss of compressed air exiting through the suction slot is minor for both slot designs with only 1.6 % (suction I) and 4.6 % (suction II) of the total captured mass flow. Because of the enhanced length of the slot, suction II is considered to be more tolerant towards any unsteadiness or modification of the simulated test conditions and is therefore recommended for the experimental testing. The conditions at the interface between isolator and combustor (cross section at half length of the central strut injector, where x = 580 mm) shown in Fig. 6 represent a strongly three-dimensional and non-uniform flow field due to the 3D intake. The average levels of pressure ($p_{av} = 0.522$ bar) and temperature ($T_{av} = 1{,}090$ K)

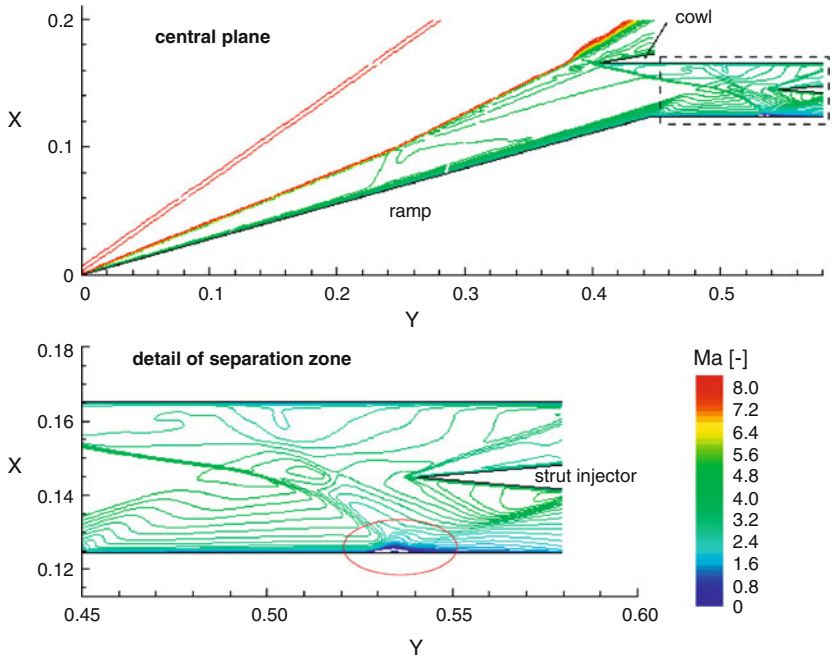

Fig. 4 Mach number distribution in the central plane of the intake (*top*) and detail of the impinging cowl shock at the *bottom* wall causing a separation zone (*bottom*)

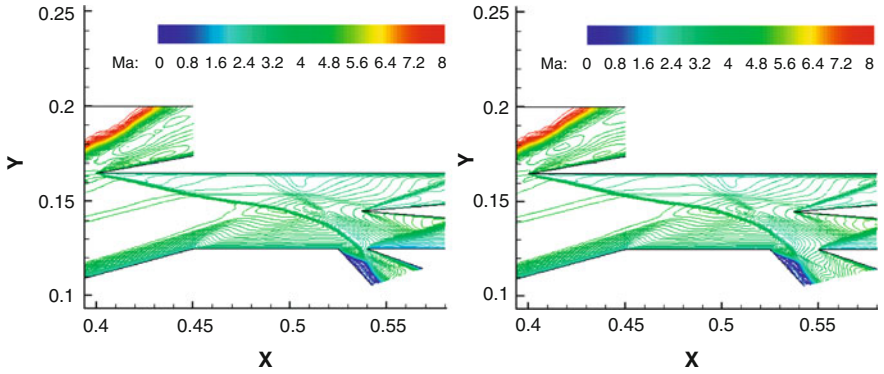

Fig. 5 Mach number distribution in the central plane for suction I (*left*) and suction II (*right*)

are relatively low, while the Mach number is high ($Ma_{av} = 3.02$). With respect to the aspired self-ignition the conditions are particularly poor in the region directly beneath the strut where the temperature is about 800 K and less. These unfavorable conditions are intensified downstream of the interface, where the divergent geometry of the combustor further accelerates the flow and decreases the level of temperature.

Table 2 Calculated air mass flows for intake simulations with passive suction

	Total ($\frac{g}{s}$)	Relative (%)
Mass flow intake $\dot{m}_{inflow}$	636	100.0
Mass flow suction I $\dot{m}_{suction\ I}$	10	1.6
Mass flow suction II $\dot{m}_{suction\ II}$	29	4.6

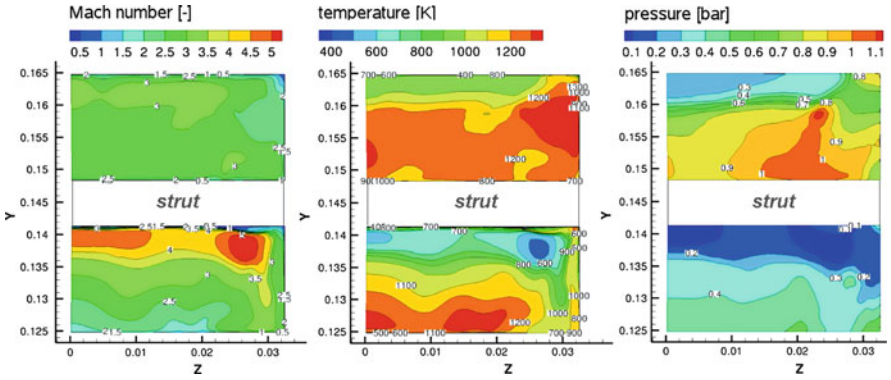

Fig. 6 Mach number (*left*), temperature (*middle*) and pressure (*right*) distribution at the cross section at x = 580 mm (interface between intake and combustor simulation), respectively

Table 3 Inflow conditions for the hydrogen injection into the combustor (horizontal and vertical ports)

	Hydrogen
Mach number Ma_{H_2} (−)	2.15
Equivalence ratio ϕ	0.6
Mass flow $\dot{m}_{H_2}$ ($\frac{g}{s}$)	10.8
Total pressure $p_{H_2,0}$ (bar)	7.0
Static pressure p_{H_2} (bar)	0.7
Total temperature $T_{H_2,0}$ (K)	293.0
Static temperature T_{H_2} (K)	145.0
Wall temperature strut T_{wall} (K)	293.0

5 Investigation of the Combustor

The conditions for the hydrogen injection are given in Table 3, the conditions for the incoming air flow at the interface are adopted from the intake simulation. In consequence of the suboptimal conditions at the interface discussed at the end of Sect. 4 and the further decrease in temperature due to the diverging combustion chamber, no self-ignition is achieved during the simulation of the combustor. In order to enforce ignition with a design change still feasible at this stage of the project, ignition wedges are integrated in the model. Placed at the top and bottom walls of the combustor close to the trailing edge of the strut injector, they are

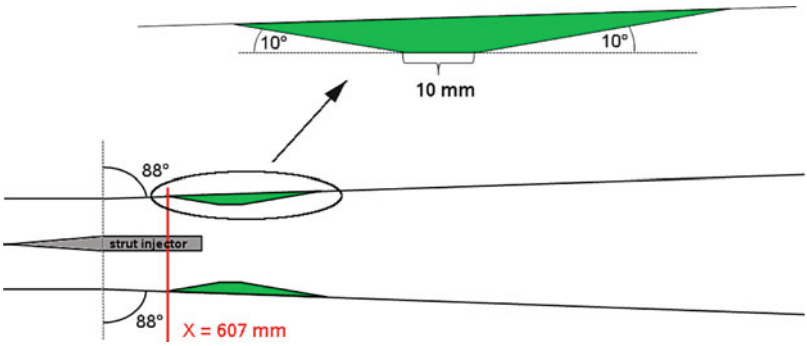

Fig. 7 Sketch of the ignition wedges and their position in the model

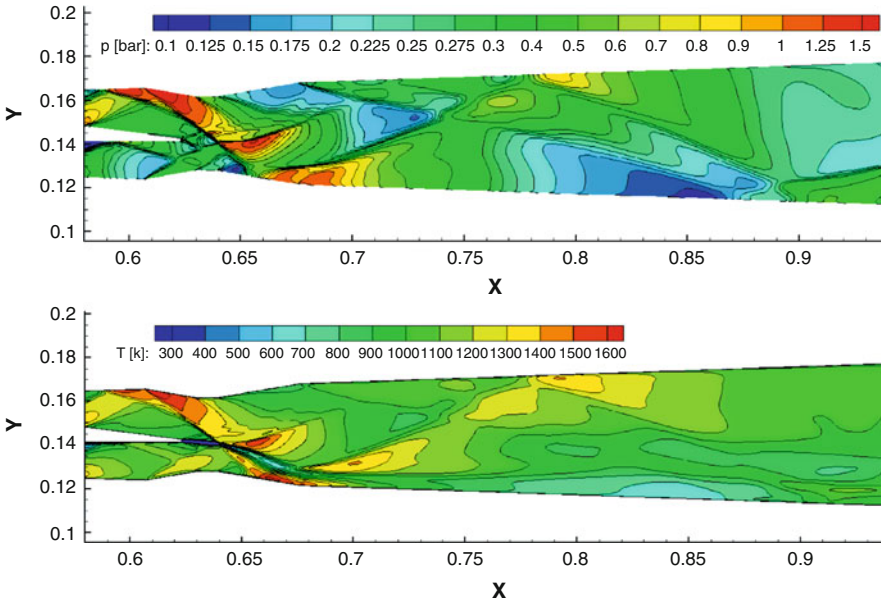

Fig. 8 Pressure (*top*) and temperature (*bottom*) distribution in the central plane of the combustor with ignition wedges (non-reactive simulation), respectively

designed to initiate a shock system that locally increases the temperature close to the injection and, thus, enables ignition. Figure 7 sketches the geometry and the position of the ignition wedges.

The evolving shock system due to the ignition wedges is observed in the pressure and temperature distributions in the central plane in Fig. 8 (non-reactive simulation). Enforced by a reflecting shock wave in the upper region of the incoming flow, the shock wave originating from the front ramp of the top wedge is more dominant than the one generated by the bottom wedge. The top wedge shock crosses the cold injected hydrogen about 16 mm downstream of the injector's trailing edge,

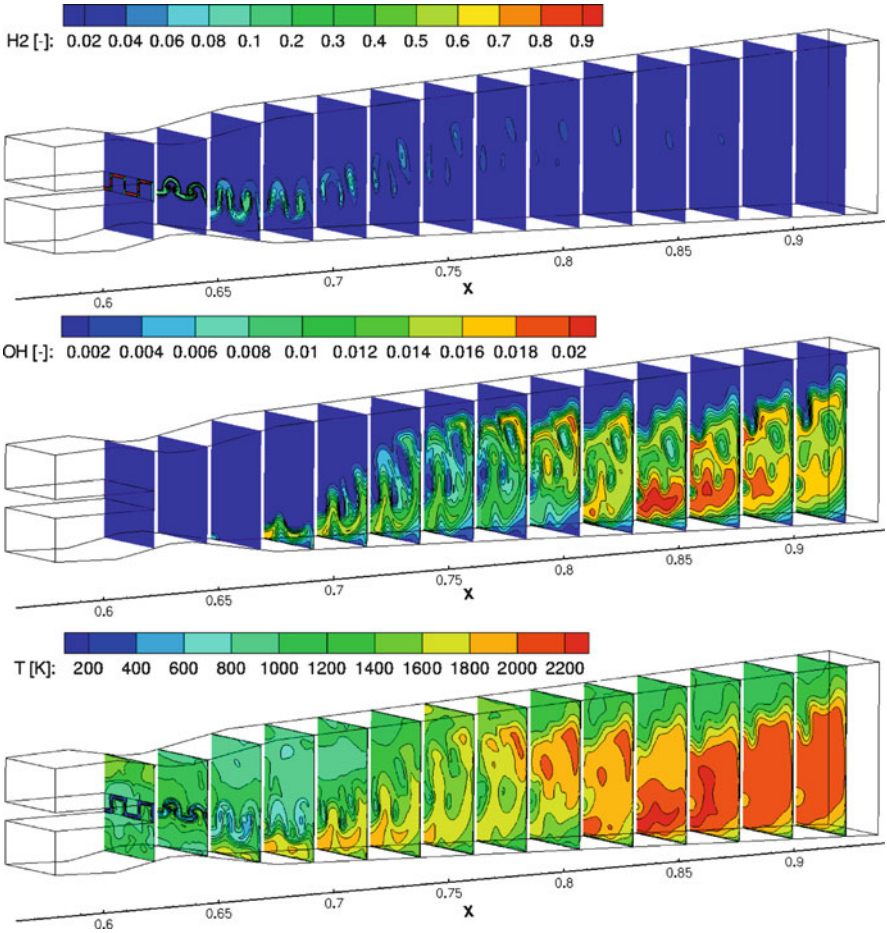

Fig. 9 H_2 (*top*), OH (*middle*) and temperature (*bottom*) distributions at cross sections of the combustor (reactive simulation), respectively

thereby deflecting the fuel towards the lower half of the combustion chamber. Further downstream the shock wave is reflected by the bottom and top walls. The temperature distribution shows three local maxima above 1,500 K: at the front ramp of the top wedge, at about 30 mm downstream of the injector and nearby the rear ramp of the bottom wedge. The upper part of Fig. 9 shows the H_2 distribution for the reacting flow at several cross sections of the model. The deflection of hydrogen by the shock waves is observed as well as the mixing of fuel and air supported by the strong vortices which are induced by the lobed strut. At the hot spot close to the rear ramp of the bottom wedge, hydrogen and air are sufficiently mixed in order to ignite. Accordingly we observe a significant increase in the temperature and OH mass fraction distributions close to the bottom wall (middle and bottom part of

Table 4 Computational performance of the simulations for the ITAM hypersonic wind tunnel experiments

	Intake	Combustor non-reactive	Combustor reactive
Number of volumes (Mio)	14.4	9.6	9.6
Number of species	2	3	9
Number of iterations	140,000	130,000	80,000 (on basis of non-reactive solution)
Vector op. ratio (%)	98.16	98.68	99.12
Average vector length	105.3	191.8	212.5
MFLOPS	4,329	4,912	7,204
Quota peak perf. (%)	4.2	4.8	7.0
Wall-clock time/iter. (s)	1.008	0.744	1.538
Total CPU time (h)	627	430	547

Fig. 9). Further downstream the flame spreads over the whole cross section and a non-uniform, detached flame develops. Therefore the simulation gives evidence of the successful use of the ignition wedges, while no thermal blockage is observed. Due to the short experimental testing times the high temperatures close to the bottom wall are not considered to be critical for the model. Numerical simulations with a reduced total temperature (inflow conditions listed in column B in Table 1) indicate very low temperatures and high Mach numbers at the interface between intake and combustor ($T_{av} = 852\,K$, $Ma_{av} = 3.14$). In spite of these unfavorable conditions, the ignition wedges again increase the temperature locally and enforce ignition.

6 Performance Analysis

The numerical investigations of the intake and the combustor have been performed on the NEC SX-9 at the High Performance Computing Center Stuttgart using 1 node and 16 CPUs. Table 4 gives an overview of the performance for the non-reactive and reactive simulations. The average vector length is longer for simulations with a high number of species. Accordingly the best vector performance is achieved by the reactive simulation of the combustor using nine species (vector operation ratio of 99.12 %). The low quotas of peak performace on the NEC SX-9 (4.2–7.0 %), particularly in comparison to the previous vector-processor based HPC, the NEC SX-8, have already been discussed in Ref. [15].

Table 5 lists the five most time consuming subroutines (using about 73.6 % of the computational time) for the reactive simulation of the combustor and their performance data. All subroutines show high vector operation ratios (98.69–99.87 %), but the performance varies between 3,413 and 11,247 MFLOPS (3.3–11.0 % peak performance) due to significant differences with regard to the bank conflicts. On the right hand side (RHS) of the set of equations subroutine PROP calculates the

Table 5 Performance data for the most time consuming subroutines for the reactive simulation of the combustor

Subroutine	Time (%)	MFLOPS	Vec. op. ratio (%)	Av. vec. length	Bank confl.	Quota peak perf. (%)
PROP	20.8	8,035	98.69	255.9	1.74	7.8
LINE3D	17.5	3,413	99.25	223.3	534.54	3.3
REACTION	16.8	11,247	99.41	240.0	22.93	11.0
LFSWEEP	9.3	3,627	99.87	219.9	647.65	3.5
UFSWEEP	9.2	3,635	99.87	219.7	647.90	3.5

gas properties and subroutine REACTION the chemical source terms. As these are local phenomena, both subroutines only depend on the data of each volume. On the contrary the implicit left hand side (LHS) of the set of equations is solved using an implicit lower-upper symmetric Gauss-Seidel solver (LU-SGS) [8, 10–12]. In order to resolve the data dependency from neighboring cells of the structured i, j, k-ordered grid the LHS subroutines LINE3D, UFSWEEP and LFSWEEP are vectorized along hyperplanes defined by $i + j + k = const.$ using indirect addressing. This probably causes memory latencies and therefore more bank conflicts per iteration (0.5345–0.6479 for the subroutines LINE3D, UFSWEEP and LFSWEEP in comparison to only 0.0017–0.0229 for the subroutines PROP and REACTION).

7 Conclusion

A complete scramjet demonstrator model designated for wind tunnel testing at Mach 8 has been investigated numerically. A separation zone evolving from the interaction of the cowl shock and the boundary layer at the bottom wall of the model has been successfully eliminated by passive suction. The mass flow exiting the model through the suction slot has been evaluated. The first simulation of the combustor showed that the conditions were to cold for self-ignition. Therefore ignition wedges have been integrated in the model. It has been shown for two different test conditions, that the evolving shock system increases the temperature locally and enables self-ignition and a stable combustion.

The performance of the simulations of the intake and the combustor on the NEC SX-9 system has been analyzed. A good vector performance has been shown, especially for the reactive simulation of the combustor. Still, the high number of bank conflicts resulting from the indirect addressing of the LHS has to be further investigated and decreased. When the experimental data is fully analyzed, further simulations reproducing the exact testing conditions have to be performed in order to compare the experimental and the numerical results quantitatively. Furthermore it is intended to port the simulations of the scramjet demonstrator model to the massive parallel scalar Cray XE6 system using more CPUs.

Acknowledgements This work has been supported by the German Research Foundation (DFG) within the GRK 1095/2. The experimental testing has been funded by the DFG grant GA 1332/1-1. The authors would like to thank Dr. Uwe Gaisbauer, Institute of Aerodynamics and Gas Dynamics, University of Stuttgart, who is in charge of the experiments of the project, for the collaboration and support. The simulations have been performed on the national super computer NEC SX-9 at the High Performance Computing Center Stuttgart (HLRS) under the grant number scrcomb.

References

1. Goonko, Y. P., Kharitonov, A. M., Mazhul, I. I., Zvegintsev, V. I., Nalivaichenko, D. G., Chirkashenko, V. F.: Investigations of a Scramjet Model at Hypersonic Velocities and High Reynolds Numbers, AIAA-paper 2002–5273, 2002.
2. Reinartz, B., Behr, M.: Computational Design Study of a 3D Hypersonic Intake for Scramjet Design Testing, High Performance Computing in Science and Engineering 2010, Springer, pp. 429–442, 2010.
3. Gerlinger, P., Stoll, P., Kindler, M., Schneider, F. and Aigner, M.: Numerical Investigation of Mixing and Combustion Enhancement in Supersonic Combustors by Strut Induced Streamwise Vorticity, Aerospace Science and Technology, **12**, pp. 159–168, 2008.
4. Kindler, M., Blacha, T., Lempke, M., Gerlinger, P. and Aigner, M.: Numerical Investigations of Model Scramjet Combustors, High Performance Computing in Science and Engineering 2008, Springer, pp. 153–166, 2008.
5. Coakley, T. J., Huang, P. G.,: Turbulence Modeling for High Speed Flows, AIAA-paper 92-0436, 1992.
6. Gerlinger, P.: Numerische Verbrennungssimulation, Springer, ISBN 3-540-23337-7, Berlin-Heidelberg, 2005.
7. Gerlinger, P.: Investigations of an Assumed PDF Approach for Finite-Rate-Chemistry, Combustion Science and Technology, **175**, pp. 841–872, 2003.
8. Gerlinger, P., Möbus, H., Brüggemann, D.: An Implicit Multigrid Method for Turbulent Combustion, Journal of Computational Physics, **167**, pp. 247–276, 2001.
9. Jachimowski, C. J.: An Analytical Study of the Hydrogen-Air Reactions Mechanism With Application to Scramjet Combustion, NASA TP-2791, 1988.
10. Shuen, J. S.: Upwind Differencing and LU Factorization for Chemical Non-Equilibrium Navier-Stokes Equations, Journal of Computational Physics, **99**, pp. 233–250, 1992.
11. Jameson, A., Yoon, S.: Lower-Upper Implicit Scheme with Multiple Grids for the Euler Equations, AIAA Journal, **25**, pp. 929–937, 1987.
12. Gerlinger, P., Brüggemann, D.: An Implicit Multigrid Scheme for the Compressible Navier-Stokes Equations with Low-Reynolds-Number Turbulence Closure, Journal of Fluids Engineering, **120**, pp. 257–262, 1998.
13. Stoll, P., Gerlinger, P., Brüggemann, D.: Domain Decomposition for an Implicit LU-SGS Scheme Using Overlapping Grids, AIAA-paper 97–1896, 1997.
14. Stoll, P., Gerlinger, P., Brüggemann, D.: Implicit Preconditioning Method for Turbulent Reacting Flows, Proceedings of the 4th ECCOMAS Conference, **1**, pp. 205–212, John Wiley & Sons, 1998.
15. Kindler, M., Gerlinger, P. and Aigner, M.: Delayed Detached Eddy Simulations of Compressible Turbulent Mixing Layer and Detailed Performance Analysis of Scientific In-House Code TASCOM3D, High Performance Computing in Science and Engineering 2011, Springer, pp. 259–272, 2011.